Research article

Microbiome transition mediated plant immune response to *Alternaria solani* (Ellis & Martin) Jones & Grout infection in tomato (*Solanum lycopersicum* L.)

Karun Wilson [a,b], Sathiavelu Arunachalam [b,*]

[a] School of Bio Sciences and Technology, Vellore Institute of Technology, Vellore, Tamil Nadu, India
[b] VIT School of Agricultural Innovations and Advanced Learning, Vellore Institute of Technology, Vellore, Tamil Nadu, India

A R T I C L E   I N F O

A B S T R A C T

Alternaria solani (Ellis & Martin) Jones & Grout, causing early blight infection in *solanaceous* crops, is a growing threat influencing sustainable crop production. Understanding the variation in the foliar microbiome, particularly the bacterial community during pathogenesis, can provide critical information on host-pathogen interactions, highlighting the host immune response during pathogen invasion. In the present study, early blight (EB) infection was artificially induced in tomato leaves, and the transition in the foliar bacterial community from healthy leaf tissue to infected leaves was analyzed. The 16s sequencing data revealed a significant shift in alpha and beta diversity, with infected leaf tissue exhibiting considerably lower bacterial abundance and diversity. Further interpretation at the genus level highlighted the possible role of the host immune system in recruiting higher nitrogen-fixing bacteria to resist the pathogen. The study, in addition to analyzing the foliar bacterial community transition during pathogenesis, has also shed light on the possible strategy employed by the host in recruiting selective nutrient-enriching microbes. Further application of this research in developing biocontrol agents with higher microbial host colonizing ability will be of tremendous benefit in achieving sustainable EB control measures.

1. Introduction

The genus *Alternaria* encompasses a group of ubiquitous necrotrophic fungal pathogens that infect a wide range of hosts [1]. Early blight disease, caused by *A. solani,* is among the most critical leaf spot diseases affecting economically important crops such as citrus, tobacco, tomato, and beans [2]. Specifically, early blight in tomatoes has led to annual economic yield losses of up to 79 percent [3]. Current control measures primarily rely on fungicides and cultural practices, which often fall short of providing sustainable and effective long-term solutions [3]. Therefore, there is an urgent need for alternative, environmentally friendly approaches to manage early blight infections.

The foliar microbiome, the community of microorganisms residing on the leaf surface, constitutes the first line of defense against pathogen invasion [4]. This microbial community plays a pivotal role in plant health by suppressing pathogen growth, enhancing plant immunity, and facilitating nutrient acquisition. Despite its importance, the community-level impact of the foliar microbiome on plant

health during pathogenesis is less understood compared to the well-studied rhizosphere microbiota.

Leaves act as filters for microorganisms from diverse environments, promoting the colonization of specific microbes that can either benefit or harm the host plant [5,6]. Keystone taxa within these communities significantly influence microbiome composition and function, and their absence can lead to severe disruptions [7]. Interactions within the foliar microbiome, including competition and antibiosis, can modify plant defense responses and influence disease [8].

Understanding the dynamics of the foliar microbiome during pathogen invasion is crucial for developing biocontrol strategies. For example, the microbial diversity of *Arabidopsis thaliana* leaves dramatically decreases when infected by a host-adapted biotrophic pathogen, underscoring the significant impact of pathogenesis on native microbial communities [9]. Plants can modulate their innate immune system in response to both beneficial and pathogenic microbes, often recruiting specific microbes that enhance their defense mechanisms [10].

Microbial interactions can activate complex plant immune responses, such as the recruitment of mycorrhizal and rhizobial associations, which enhance phosphorus and nitrogen uptake [11]. Nitrogen deficiency increases plant susceptibility to necrotrophic fungal pathogens, including *A. solani* [12]. Although many studies have investigated microbiome changes in infected versus healthy plants, the mechanisms driving these changes remain largely unexplored.

This study aims to elucidate the significance of the foliar microbiome in countering pathogen invasion, focusing on the modulation of the native microbial community to enhance plant immunity. Specifically, examining the impact of early blight infection on the foliar bacterial community of tomato leaves, exploring the potential role of the microbiome in disease suppression and the host plant's recruitment of nutrient-enriching microbes. By providing insights into these interactions, the study aims to contribute to the development of sustainable biocontrol agents with enhanced microbial colonization abilities, ultimately benefiting crop production and plant health.

2. Materials and methods

2.1. Experimental design

In 2023, the fungal strain *A. solani* was isolated from symptomatic tomato crops in the Vellore Institute of Technology's agricultural field (GPS coordinates: 12°58′04.5″N, 79°09′38.0″E). The culture was grown in potato dextrose agar (PDA), and the produced spores were stored in glycerol stock for further research.

Tomato variety PKM-1, which is susceptible to early blight infection, was selected for the study. Seedlings were grown in a seed tray for up to 14 days and later transferred to four individual pots with two seedlings each. Sterile red soil was used as a substrate in both the seedling tray and pots. The fungal culture was grown in PDA media over 12 days to obtain sufficient spores. The spore suspension was adjusted to 2×10^5 spores/mL using a hemocytometer, followed by the addition of 0.01 percent Tween 20 to act as a surfactant [13]. Following 30 days post-transplantation, the experiment was carried out using one control pot and three experimental pots. The healthy lower individual leaves of the three experimental pots (six plants) were sprayed with spore suspension, while the upper leaves remained untreated. To enhance the infection, adequate ambient moisture was maintained for 4 h.

After 24 days post-inoculation, disease severity in all three pots was evaluated. Leaves displaying lesions covering at least 40 percent of the leaf area were collected from each pot as a single sample, designated as "AS-01". To confirm the presence of *A. solani* infection, a portion of the symptomatic leaves was inoculated onto PDA media. Additionally, leaf samples were collected from the healthy upper leaves of the experimental pots and labeled as "TH-01". Both *A. solani* infected leaf sample (AS-01) and the healthy leaf sample (TH-01) were further processed for analysis.

2.2. Extraction of DNA, 16S amplification, and high-throughput sequencing

DNA extraction was performed using the commercially available QIAGEN soil kit following the manufacturer's protocol (https://www.qiagen.com/au/resources). The concentration and quality of DNA were determined using the NanoDrop with readings at 260/280 nm showing a value of 1.8–2. To amplify the 16S bacterial region, primer pairs V13F (5′ AGAGTTTGATGMTGGCTCAG 3′) and V13R (5′ TTACCGCGGCMGCSGGCAC 3′) were used [14]. The polymerase chain reaction was performed with 40 ng of extracted DNA, 10 pM of each primer, and Xploregen discoveries Taq Master mix. The master mix was composed of high-fidelity DNA polymerase, 0.5 mM dNTPs, 3.2 mM MgCl$_2$, and PCR enzyme buffer. The polymerase chain reaction conditions included initial denaturation at 95 °C, followed by 25 cycles of denaturation at 95 °C for 15 s, annealing at 60 °C for 15 s elongation at 72 °C for 2 min, a final extraction at 72 °C for 10 min, and a hold at 4 °C [15]. The amplified products were purified and assessed using a 2 percent agarose gel and Nanodrop QC analysis. Unused primers were removed with the help of AMPure XP beads on each amplicon sample, followed by the preparation of sequencing libraries by an additional eight cycles of PCR, using Illumina barcoded adapters. Purification of libraries was performed using AMPure beads and Qubit dsDNA high sensitivity assay kit for quantitation. Sequencing was performed using Illumina Miseq with 2 × 300 PE v3 sequencing kit.

2.3. Sequence data processing

Quality control of raw data was performed using FASTQC (v0.11.2) [16] and MULTIQC (v1.9) [17], followed by TRIMGALORE for trimming low-quality reads and adapters [18]. Trimmed reads were further processed by merging paired-end reads, chimera removal, and operational taxonomic unit (OTU) abundance calculation. Picking of representative sequences, estimation correction, and

taxonomic classification were done using Biokart Pipeline, enabling high-precision investigations at the genus level. SILVA [18], GREENGENES [19], and NCBI [20] databases were used based on the identity and percentage coverage of each read. The raw data have been deposited in NCBI's Sequence Read Archive (SRA) database with BioSample accessions SAMN32691190, SAMN32691191.

2.4. Statistical analyses

The R statistical platform version 4.0.4 (R Foundation for Statistical Computing, Vienna, Austria) was used to perform statistical analyses and calculations. To assess the variation in bacterial diversity under the influence of *A. solani*, alpha-diversity indexes including the Shannon index [21], Chao1 index [22], and observed richness [23] were assessed. To visualize the relative abundance of top bacterial genera in the samples, a heatmap was generated using the OTU count. The data were normalized using MinMaxScaler from the scikit-learn library to scale the abundance values between 0 and 1 [24]. The heatmap was plotted using the seaborn library in Python. Relative abundance percentage of the overall microbial community and specifically *Nitrospira* in the samples were pivoted based on taxonomic levels using Microsoft Excel 2010. The DCA (Detrended Correspondence Analysis) and Abundance-occupancy plots were created using the Matplotlib library of Python scripting language [25]. The DCA plot visualizes the taxonomic composition and distribution of bacterial communities associated with TH-01 and AS-01. Abundance-occupancy plots visualize the x-axis representing the abundance of microbial taxa, displayed on a logarithmic scale, and the y-axis representing the occupancy of microbial taxa [26].

The co-occurrence network was generated using the NetworkX library in Python with the top ten genera with higher OTU count and interactions among AS-01 and TH-01 [27]. A graphical representation was created where each genus has a node connected by edges based on their co-occurrence patterns. Node size reflected OTU count in AS-01, emphasizing genus abundance, while lines between nodes represented strong and significant correlations. Additionally, the Circos plot was generated using the NetworkX library, visualizing network structure in a circular ideogram format via Matplotlib [28]. This facilitated a deeper understanding of microbial co-occurrence among the top genera.

The core microbiome analysis was conducted using the Python programming language, using the Pandas library for data manipulation and Seaborn for heatmap visualization [24]. The primary parameters set for the analysis included selecting genera with a minimum count of one in both samples, sorting genera based on the sum of counts across samples, and limiting the analysis to the top 50 OTUs. The heatmap was generated with annotations enabled to display the count values for each genus in the two samples. Additionally, the colormap 'YlGnBu' was chosen to represent the abundance levels of the genera in the heatmap, providing a visually informative representation of the core microbiome composition across the samples.

A comparative study was conducted to analyze the variations in OTU counts within a selected genus. A Venn diagram was created using the 'VennDiagram' package, illustrating a clear transition of microbial communities in samples [29]. The microbial community in early blight-infected leaves was assessed against healthy leaves to understand the ecological functions of varying bacterial abundance and their role in the plant's immune response to pathogens. Relative abundance of individual taxa was calculated using the following formula:

$$R(I) = \left(N(i) \middle/ \sum [N(J)] \right) \times 100$$

Where the summation $\sum$ is taken over all species (j = 1 to n)

$N(i)$ represents the number of individuals of the ith species

$\sum [N(J)]$ represents the sum of the number of individuals across all species in the sample

$R(I)$ represents the relative abundance of the ith species, expressed as a percentage

3. Results

This study explores how *A. solani* infection affects foliar bacterial diversity in tomato plants, aiming to elucidate the plant's immune response and its impact on leaf microbiota. The results revealed a significant shift in the composition and abundance of the native microbial community following infection. Infected leaves exhibited a notable reduction in bacterial diversity and population size compared to healthy ones, indicating a disruption in the leaf microbiota equilibrium in response to pathogenic invasion. Additionally, the findings suggest that quorum sensing and microbe-associated molecular patterns (MAMPs) may trigger pattern-triggered immunity (PTI) responses, highlighting the complex interplay between plant immunity and microbial dynamics. The study offers insights into the mechanisms driving plant-microbe interactions during early blight infection, shedding light on the adaptive strategies employed by both host plants and associated microbiota to combat pathogenic threats. These findings have implications for understanding plant immune responses and developing sustainable disease management strategies in agriculture.

3.1. Taxonomic composition and diversity of the bacterial community

A detailed analysis of the taxonomic composition and diversity of the foliar bacterial community was performed to understand how *A. solani* infection influences microbial dynamics in tomato plants. The dataset, comprising 800,000 high-quality 16s reads from two samples (TH01 and AS01), enabled the identification of 14,852 Operational Taxonomic Units (OTUs). These OTUs were taxonomically classified into 125 genera spanning 18 phyla, providing a comprehensive view of the leaf microbiota. Notably, the genus *Nitrospira* was prevalent, accounting for over 30 percent of the sequences, indicating its dominance within the microbial community. Furthermore,

analysis of the top seven most dominant OTUs revealed the ubiquity of *Nitrospira* across both healthy and infected samples (Fig. 1).

Further analysis unveiled noticeable patterns of bacterial distribution between healthy and infected leaves, highlighting the influence of *A. solani* infection on microbial diversity. Among the 125 bacterial genera analyzed, 19 (15.2 %) were exclusively present in infected leaves, while 40 (32 %) were unique to healthy ones, indicating a notable divergence in bacterial composition. Despite these differences, both infected and healthy leaf samples shared the same genera 66 (52.8 %) as shown in Fig. 2 and as Ven diagram in Fig. 3 (A). Both samples had the presence of bacterial genera, *Nitrospira* and *Bacillus* that are known for their antifungal properties. This suggests a potential role in host defense mechanisms against *A. solani* infection.

3.2. Assessment of alpha diversity

The α-diversity indexes were conducted to assess within-sample bacterial community diversity in healthy and early blight-infected leaves. Triplified analyses provided insights into the richness and evenness of microbial populations within each sample. In Fig. 3 (A–D), utilizing metrics such as Fig. 3 (B) Shannon index, Fig. 3 (C) Chao1 index, and Fig. 3 (D) Observed richness, α-diversity was quantified, with whisker box plots illustrating the observed value range. Remarkably, healthy leaf samples exhibited greater bacterial diversity across all metrics compared to infected leaves, indicating a disruption of ecological balance in response to pathogenic invasion.

The disparity in bacterial diversity between healthy and infected leaf samples highlights the profound impact of *A. solani* infection on microbial community structure within tomato foliage. Elevated α-diversity metrics in healthy leaves signify a robust and resilient microbiome capable of withstanding environmental pressures. Conversely, reduced α-diversity in infected leaves suggests a perturbation in microbial equilibrium, indicative of compromised host-pathogen interactions.

3.3. Assessment of β-Diversity

The β-diversity analysis was performed between-sample diversity and delineated microbial community composition differences between healthy and infected leaf samples. The Principal Coordinate Analysis (PCoA) plot Fig. 4, revealed significant divergence in microbial community clusters, with distinct clusters representing unique compositional profiles shaped by infecting pathogens. The 2D plot generated with Axis 1 representing the highest level of variation and Axis 2 indicating the subsequent highest dimension of variation. The heatmap (Fig. 5) displays the relative abundance of the top 17 bacterial genera identified in the infected (AS01) and healthy (TH01) tomato leaf samples. The genera are on the y-axis and the sample types (AS01 and TH01) on the x-axis. The color gradient ranges from blue to red, representing the lowest to highest abundance, respectively. Genera such as *Nitrospira, Candidatus Kuenenia*, and *Paracoccus* were notably more abundant in both samples, while some genera like *Bifidobacterium* were significantly less abundant in the infected sample. This visualization highlights the shifts in microbial community composition in response to *A. solani* infection.

Beta diversity is represented through a Principal Coordinate Analysis (PCoA) plot portraying significant differences in the microbial community between AS01 and TH01. Each axis representing the percentage of variation between the samples and the colored points depicts the interrelationship between different groups of OTUs based on their unique characteristics and source.
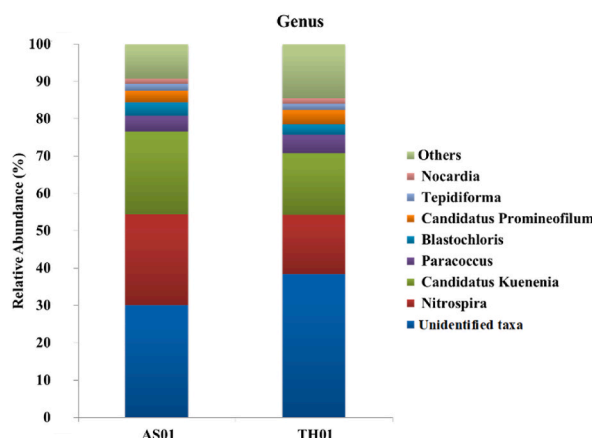
A Detrended Correspondence Analysis (DCA) plot

Fig. 1. Graphical representation of relative bacterial abundance.
The figure represents the variation of bacterial abundance observed in AS01 (*A. solani* infected) and TH01 (healthy leaf sample) portraying variation in the community structure during early blight infection. Different colors correspond to the major genus residing in the sample, at varying proportions.

Exclusively present in "TH01"
Achromobacter, Alistipes, Anaerostipes, Arcobacter, Blattabacterium, Bosea, Brevefilum, Candidatus Cloacimonas, Candidatus Hodgkinia, Cupriavidus, Desulfallas, Desulfovibrio, Dysosmobacter, Egicoccus, Elizabethkingia, Escherichia, Exiguobacterium, Fibrobacter, Flavobacterium, Fuerstia, Gemmata, Hypericibacter, Immundisolibacter, Luteimonas, Minicystis, Morganella, Mycolicibacterium, Olsenella, Opitutus, Panacibacter, Paraflavitalea, Phascolarctobacterium, Pseudolabrys, Saccharomonospora, Solitalea, Sphingobacterium, Sphingosinicella, Stenotrophomonas, Streptococcus, Treponema.
Mutually present microbes in "TH01" and "AS01"
Acinetobacter, Akkermansia, Alkalilimnicola, Anoxybacillus, Azoarcus, Azospirillum, Bacillus, Bacteroides, Bdellovibrio, Bifidobacterium, Blastochloris, Blautia, Brevundimonas, Candidatus Babela, Candidatus Kuenenia, Candidatus Nucleicultrix, Candidatus Promineofilum, Candidatus Protochlamydia, Candidatus Solibacter, Chryseobacterium, Chryseolinea, Clostridioides, Clostridium, Conexibacter, Desulfoglaeba, Enterococcus, Faecalibacterium, Faecalitalea, Fusobacterium, Gemmatimonas, Hyphomicrobium, Ignavibacterium, Lachnoclostridium, Lactobacillus, Luteitalea, Mannheimia, Meiothermus, Mesorhizobium, Methylocystis, Mycobacterium, Niabella, Nitrosomonas, Nitrospira, Nocardia, Oscillibacter, Paludisphaera, Paracoccus, Pelolinea, Prevotella, Proteus, Pseudomonas, Pseudorhodoplanes, Rhodococcus, Rhodoplanes, Rickettsia, Ruminococcus, Sorangium, Sphingobium, Sphingomonas, Sphingopyxis, Staphylococcus, Streptomyces, Tepidiforma, Turicibacter, Unclassified.
Exclusively present in "AS01"
Acidimicrobium, Actinomyces, Aureimonas, Chelatococcus, Chitinophaga, Chloroflexus, Collinsella, Devosia, Dialister, Hoyosella, Lentibacillus, Lysobacter, Megasphaera, Methylovirgula, Micromonospora, Nitratireductor, Parageobacillus, Phenylobacterium, Rhizobium.

Fig. 2. Comparative analysis of the bacterial diversity in samples.
Sample-based comparison of bacterial genera that are either present exclusively on TH01- shaded in green or AS01- shaded in brown, and present on both samples regardless of *A. solani* infection-shaded with yellow colour.

The DCA plot was analyzed to elucidate the distribution patterns of bacterial genera across the three axes. Each data point on the plot represented a genus, allowing for the visualization of taxonomic abundance and sample clustering based on their bacterial composition.

The DCA plot revealed distinct clustering patterns of bacterial genera across AS01 and TH01 along the three axes. *Candidatus Promineofilum, Paracoccus,* and *Nocardia* are positioned very close to each other in both samples AS01 and TH01, it suggests that these genera share similar niche and can thrive in conditions present in both AS01 and TH01. However, *Nitrospira,* positioned far from the TH01 and *Candidatus Promineofilum* positioned far from the AS01 might be less adapted to the conditions present in the corresponding sample. This could be due to factors like nutrient availability, the presence of competitors, or even the early blight infection itself if it's detrimental to that particular genus.

3.4. Co-occurrence network analysis

The Co-occurrence network analysis Fig. 6 (B) revealed intricate relationships among the top 10 genera with higher OTU counts and interaction among AS01 and TH01. Following the Python script, *Candidatus Promineofilum, Blastochloris, Nitrospira, Paracoccus, Bdellovibrio, Methylocystis thylocys, Nitrosomonas, Candidatus Kuenenia,* and *Nocardia* genera were identified and represented as nodes in the network, with edges connecting pairs based on their co-occurrence patterns. The size of each node reflected its OTU count, providing a visual representation of genus abundance. Unidentified taxa had the largest node followed by *Nitrospira* and *C. Kuenenia,* and the smallest node was found to be associated with *Methylocystis.* lines were connected between the nodes to signify strong and significant correlations. This visualization offered comprehensive insights into the co-occurrence patterns and interactions within the microbial community, highlighting the complex relationships among the top 10 genera.

3.5. Abundance occupancy relationship

The abundance-occupancy plot Fig. 7 (A) provided insights into the distribution patterns of microbial genera across AS01 and TH01. Each data point on the plot represents a microbial genus, with its abundance (log scale) plotted against its occupancy (presence/absence) in the samples. The plot revealed varying distribution patterns among the microbial genera in AS01 and TH01. AS01 displayed higher microbial abundance levels compared to TH01 across the data points, with points clustered towards higher abundance values along the log scale axis. In contrast, TH01 exhibited more variability in occupancy, with some genera showing lower occupancy despite moderate to high abundance levels. This variability suggests spatial heterogeneity in the distribution of TH01 genera, with certain taxa being more localized or niche-specific in their habitat preferences.
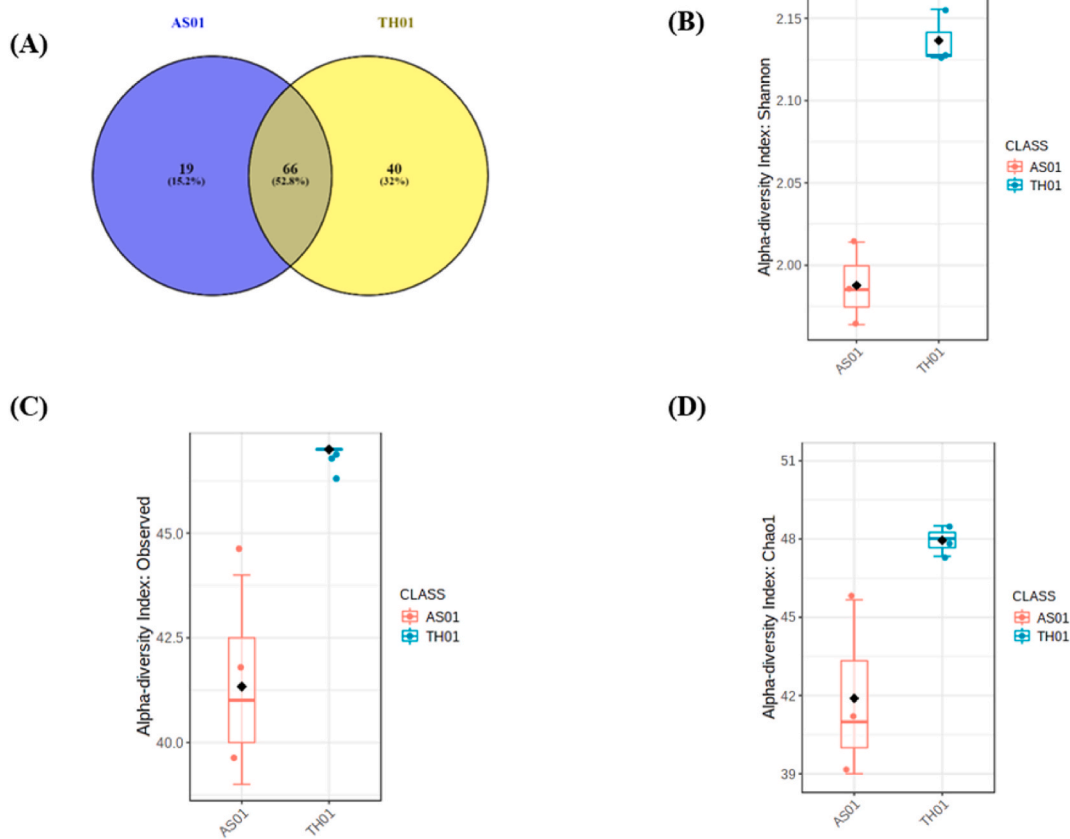
Fig. 3. Microbiome distribution, and Alpha-diversity Index.
(A) Ven diagram representing percentage distribution of OTUs in infected and healthy leaf projecting unique, and mutually shared microbial community. Alpha diversity indexes are represented through **(B)** Shannon index; **(C)** Chao1 index and **(D)** Observed richness portraying decreased bacterial diversity in the infected leaf compared to healthy tissue.
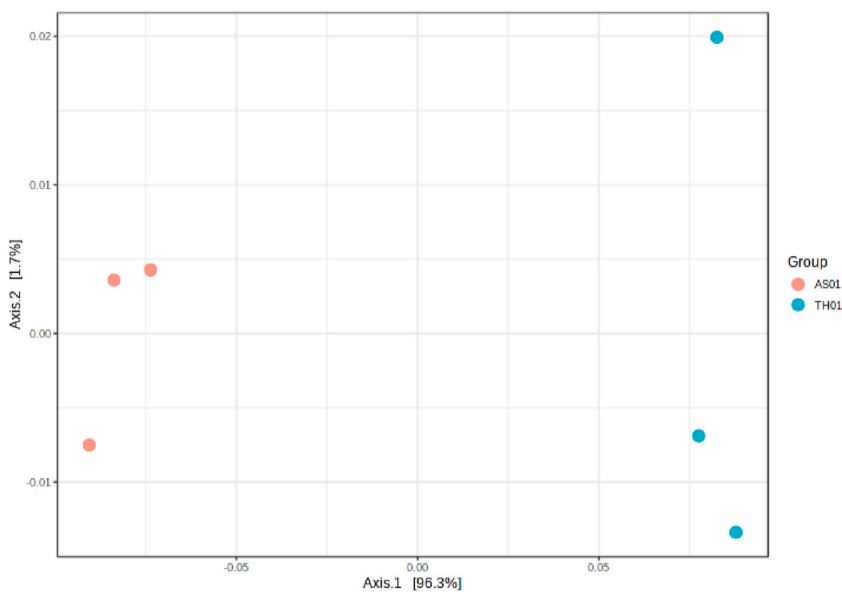

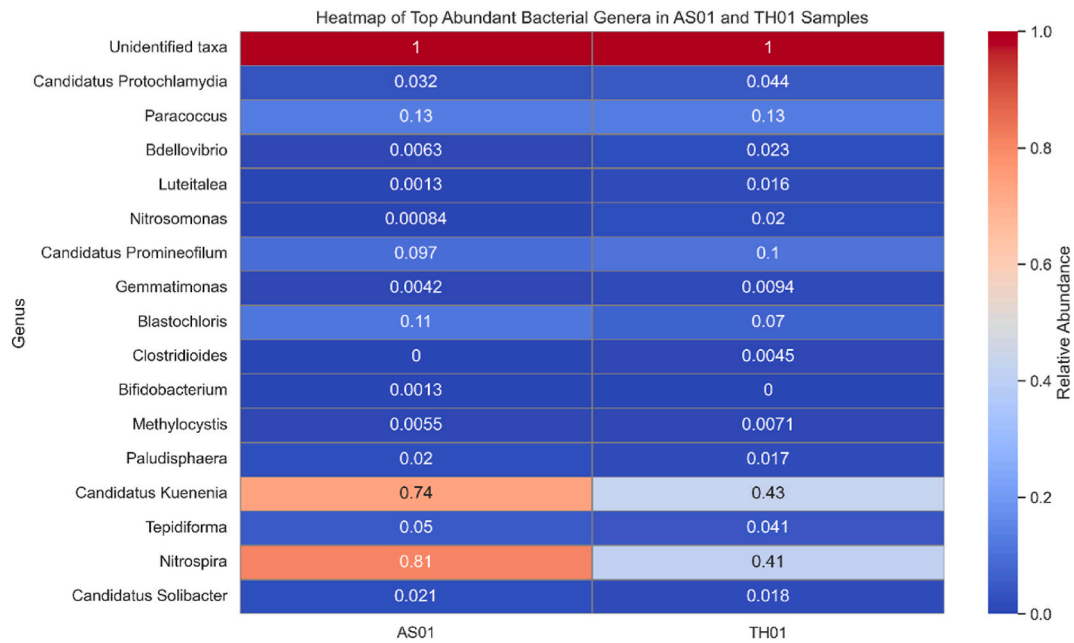**Fig. 4.** Beta diversity of AS01 and TH01.

Fig. 5. Heatmap of the relative abundance of the top 17 bacterial genera in infected (AS01) and healthy (TH01) tomato leaf samples. The color gradient ranges from blue (lowest abundance) to red (highest abundance), illustrating the changes in microbial community composition due to *A. solani* infection. Genera such as *Nitrospira, C. Kuenenia*, and *Paracoccus* were more abundant in both samples, while *Bifidobacterium* showed a marked decrease in the infected sample.
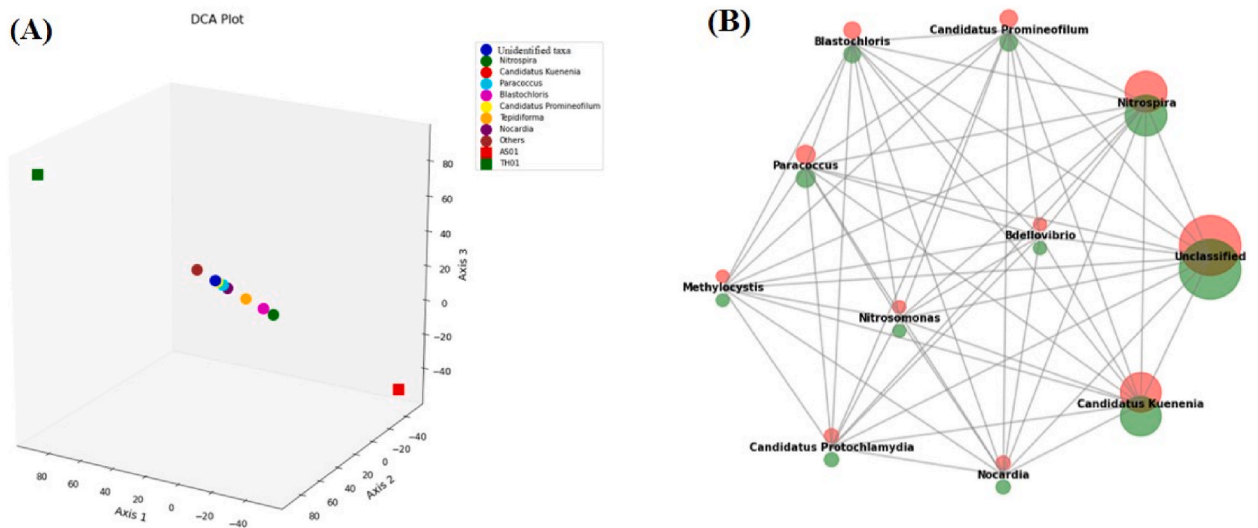

Fig. 6. (A) DCA plot depicts bacterial genus distribution across AS01 and TH01, showing clustering patterns and niche similarities among *Candidatus Promineofilum, Paracoccus*, and *Nocardia*. **(B)** Co-occurrence network analysis reveals complex interactions among top genera in AS01 and TH01, providing insights into microbial community dynamics.

3.6. Core microbiome

The core microbiome of samples AS01 and TH01 was analyzed to identify the prevalent microbial genera present across both samples. The heatmap visualization, Fig. 7 (B) illustrates the abundance of these top genera identified in both samples including Unidentified taxas, *Nitrospira, C. Kuenenia, Paracoccus, Blastochloris, C. Promineofilum, Tepidiforma*, and *Nocardia*. Among these, Unidentified taxa exhibits the highest abundance in both samples, with *Nitrospira* and *C. kuenenia* following closely behind. Overall, the heatmap provides a comprehensive overview of the core microbiome composition in samples AS01 and TH01, highlighting the dominant genera shared between the two samples. Further analysis and comparison of these genera could offer valuable insights into
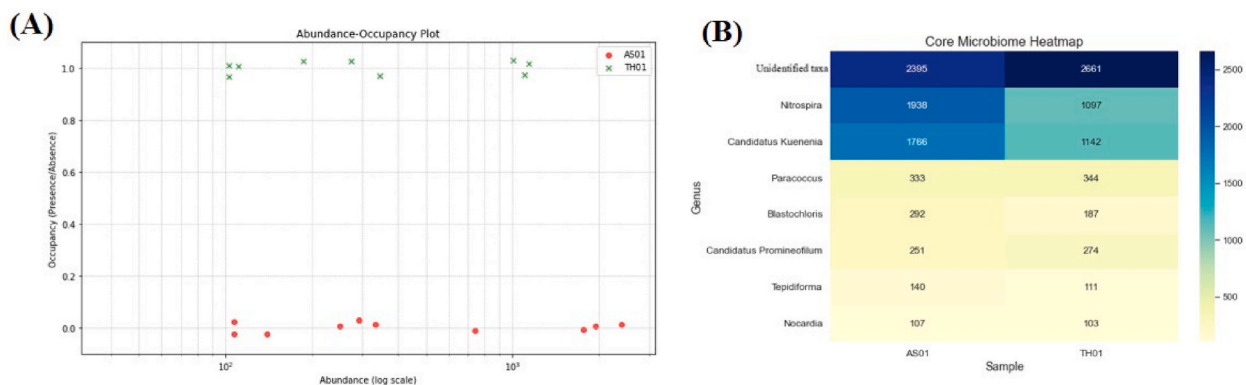
(A)

(B)

Fig. 7. (A) The abundance-occupancy plot illustrates microbial distribution patterns across AS01 and TH01, with AS01 displaying higher abundance levels. TH01 exhibits variability in occupancy, suggesting niche-specific habitat preferences among microbial genera. **(B)** Core microbiome analysis heatmap reveals dominant genera shared between AS01 and TH01, with Unidentified taxa prevailing. *Nitrospira* and *C. kuenenia* signify significant microbial community dynamics. The shade of blue darkens with increasing OTU counts, while lighter shades of yellow represent fewer OTUs.

the microbial community structure and its potential implications in the respective environments.

3.7. Circos plot

The Circos plot was constructed to visualize the relationships between key microbial genera within the foliar microbial community. Each genus was represented as a segment along the circular ideogram, with connecting links denoting their interactions based on OTU counts. Notably, the "Unclassified" genus exhibited the most prominent association, depicted by thick violet-colored links, indicating its pervasive presence and potentially significant role within the community. Following closely, "*Nitrospira*" displayed robust connections in Kelly Green, indicative of its substantial influence. "*C. Kuenenia*" appeared in yellow, reflecting its moderate associations, while "*Paracoccus*" was depicted in blue, signifying its distinct yet interconnected presence. Additionally, "*Blastochloris*" and "*C. Promineofilum*" were observed in brown and yellow-green, respectively, suggesting their noteworthy interactions. "*Tepidiforma*" appeared in dark violet, hinting at its specific relationships, while "*Nocardia*" displayed the thinnest links in mint green, underscoring its more subtle interactions within the microbial network. This comprehensive visualization provided insights into the complex interplay and potential functional roles of these key genera in shaping the gastrointestinal microbiome, contributing valuable insights to the understanding of microbial community dynamics.

Table 1
Genus sharing higher bacterial abundance in TH01 compared to the infected sample AS01.

Genus	TH01 (OTU)	AS01 (OTU)
Akkermansia	32	15
Bacteroides	17	1
Bdellovibrio	63	36
Candidatus Babela	46	10
Candidatus Promineofilum	274	251
Candidatus Protochlamydia	118	96
Chryseolinea	24	15
Clostridium	35	16
Enterococcus	6	1
Fusobacterium	24	3
Legionella	11	2
Luteitalea	43	24
Meiothermus	6	2
Mesorhizobium	17	9
Nitrosomonas	54	23
Oscillibacter	7	2
Paracoccus	344	333
Rickettsia	10	2
Sorangium	34	32
Prevotella	15	1
Bacillus	10	5
Pseudomonas	19	4
Azospirillum	20	11

3.8. Increased OTU count in nitrogen fixation bacteria

The relative abundance of bacteria in 15 distinct genera was found to be considerably higher in the infected sample compared to the healthy leaf sample based on the OTU count. Variations in relative abundance were observed in genera that include *Blastochloris*, which varied between TH01-187 and AS01-292, where 187 and 292 correspond to the number of sequence reads of each OTU. Similarly, in *Gemmatimonas*, bacterial abundance varied from TH01-26 to AS01-31, *Methylocystis* from TH01-20 to AS01-34, *Nitrospira* from TH01-1097 to AS01-1938, *Rhodococcus* from TH01-19 to AS01-21, *C. kuenenia* from TH01-142 to AS01-1766, *C. solibacter* from TH01-49 to AS01-170, *Nocardia* from TH01-103 to AS01-107, and *Ruminococcus* from TH01-1 to AS01-12, which are considered important nitrogen fixers. Additionally, variation was also found in *Tepidiforma* from TH01-111 to AS01-140, *Anoxybacillus* from TH01-3 to AS01-8, *Bifidobacterium* from TH01-1 to AS01-24, *Blautia* from TH01-1 to AS01-10, *Clostridioides* from TH01-13 to AS01-21, and *Paludisphaera* from TH01-47 to AS01-68, of which the functional aspect is uncertain. Conversely, the OTU count was lower in AS01 compared to TH01 for 22 genera (Table 1), indicating a reduction in these bacteria in the infected sample.

4. Discussion

The traditional disease triangle, consisting of virulent pathogens, susceptible hosts, and the abiotic environment, is a key concept in plant pathology [30]. However, recent studies highlight the vital role of the plant microbiome in maintaining plant health and combating disease [31]. Native antagonistic microbes within the plant microbiome can counteract pathogenic effects, which is especially important for plants lacking inherent genetic resistance to necrotrophic pathogens [32]. This is particularly evident in solanaceous crops, where susceptibility to *Alternaria* spp. leads to significant economic losses due to brown spot formation [2]. Early blight, caused by *A. solani*, remains a challenge, typically managed through cultural practices, fungicides, and resistant varieties [33]. Despite these efforts, achieving effective control without synthetic fungicides is difficult, emphasizing the need to understand the microbiome's role in disease resistance.

4.1. Taxonomic composition and diversity of the bacterial community

The study shows a notable change in foliar bacterial diversity in response to *A. solani* infection, aligning with previous studies demonstrating pathogen-induced shifts in microbial community structure [34]. The reduced species richness and diversity in infected leaves (Fig. 3B, C, D) match the observations of Remus-Emsermann and Schlechter [35], who highlighted the importance of microbial interactions in shaping the phyllosphere microbiome. The disruption of these interactions by pathogen invasion aligns with Cordero and Datta [36] findings on how such disturbances can alter community structure. The distinct clustering patterns seen in Fig. 6A reflect underlying ecological dynamics influenced by plant health, clearly differentiating healthy and infected samples. This underscores the impact of *A. solani* on foliar microbial diversity and highlights microbial dynamics' potential role in modulating plant immune responses and disease progression [37].

Co-occurrence network analysis (Fig. 6B) reveals complex interactions among the top genera in AS01 and TH01, providing insights into microbial community dynamics. Studies have shown that co-occurrence networks can elucidate relationships among microbial taxa and their functional roles within an ecosystem [38]. The abundance-occupancy plot (Fig. 7A) illustrates the distribution patterns of microbial genera across AS01 and TH01, showing higher microbial abundance levels in AS01 compared to TH01, with notable variability in occupancy. This aligns with findings by Shade and Stopnisek [39], who reported that abundance-occupancy relationships can indicate ecological strategies of microbes under stress conditions. The core microbiome analysis (Fig. 7B) highlights the dominant genera shared between AS01 and TH01, with Unidentified taxa prevailing. *Nitrospira* and *Candidatus kuenenia* signify significant microbial community dynamics. Core microbiomes often consist of stable and functionally important microbial taxa that contribute to the host's health [40]. The Circos plot (Fig. 8) illustrates intricate interactions among key microbial genera in the foliar microbiome, with thicker connecting links indicating stronger associations, unveiling complex network dynamics and potential functional roles of these genera. Such visualizations are critical for understanding microbial community structure and function in response to environmental changes [41].

4.2. Increased OTU count in nitrogen-fixing bacteria

The significant variations in nitrogen-fixing bacterial abundance between infected and healthy leaves suggest a reorganization of the plant's microbial community during pathogenesis. Similar trends have been reported, with invasive species either being eliminated or native species adapting new control mechanisms in complex environments [42]. The nitrogen-fixing capabilities of genera such as *Blastochloris, Methylococcus*, and *Nitrospira* are well-documented. For example, *Blastochloris* genomes contain genes crucial for nitrogen fixation, including Mo/Fe and Fe/Fe enzymes [43]. *Gemmatimonas* aids nitrogen fixation through its genes for various nitrogen cycles, indirectly supporting N2 fixation [44]. Type II methanotrophs, including *Methylococcus*, have demonstrated nitrogen-fixing abilities [45]. *Nitrospira*, a diverse group of nitrite-oxidizing bacteria, possesses pathways for both nitrite and ammonia oxidation, contributing to complete nitrification [45]. The nitrogen fixation capacities of *R. qingshengii* and other species within the genus further underscore the importance of nitrogen-fixing bacteria in plant health [46] The roles of *C. kuenenia* in global nitrogen cycles and *C. solibacter* in carbon cycles are significant [47,48]. Moreover, *Nocardia* species, such as *Nocardia calcarea*, contribute to atmospheric nitrogen fixation, providing insights into nitrogen delivery and resistance to early blight [49–51].

Interestingly, key biocontrol microbes such as *Bacillus, Pseudomonas*, and *Azospirillum* were less abundant in infected leaves,
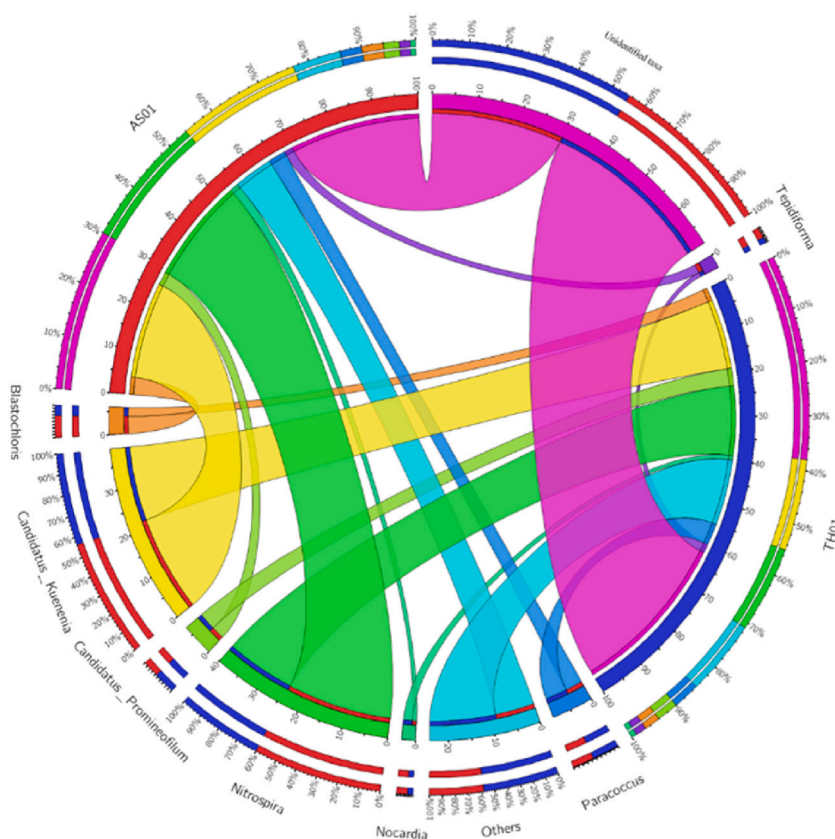
Fig. 8. The Circos plot illustrates intricate interactions among key microbial genera in the foliar microbiome, with thicker connecting links indicating stronger associations. This visualization unveils the complex network dynamics and potential functional roles of these genera within the microbial community.

suggesting a shift in microbial strategy under pathogen load. This variation in OTU count during pathogenesis may represent an alternative plant defense strategy, enhancing immune responses when primary defenses are compromised [37,52]. Lower nitrogen levels in plants are associated with increased susceptibility to *A. solani* infection, whereas high nitrogen content delays ripening and prolongs vegetative growth, thereby reducing susceptibility to early blight [49–51].

In conclusion, the selective increase in nitrogen-fixing bacteria during pathogenesis highlights an alternative plant defense mechanism, strengthening immune responses when primary defenses are weakened. This study sheds light on the complex interactions between microbial communities and plant health, offering valuable insights into host-microbe interactions and plant defense mechanisms. These findings underscore the potential for leveraging the plant microbiome in developing sustainable agricultural practices and enhancing crop resilience against pathogens.

5. Conclusion

This study elucidates the significant impact of *A. solani* infection on the foliar bacterial diversity of tomato plants. A marked reduction in bacterial diversity and population size in infected leaves was observed, indicating a disruption in leaf microbiota equilibrium due to pathogenic invasion. The findings suggest that quorum sensing and microbe-associated molecular patterns (MAMPs) may trigger pattern-triggered immunity (PTI), highlighting the intricate interplay between plant immunity and microbial dynamics.

The investigation sheds light on the intricate dynamics of plant-microbe interactions during early blight infection in tomato plants. By examining the taxonomic composition and diversity of the foliar bacterial community, the study uncovered significant shifts in microbial populations in response to *A. solani* invasion. These findings underscore the vital role of native antagonistic microbes in mitigating the adverse effects of pathogens. A discernible decline in species richness and diversity in infected leaves was observed, along with alterations in overall community composition. This disruption in microbial equilibrium highlights the impact of pathogen invasion on species interactions and community structure.

Moreover, the study reveals the strategic recruitment of specific nutrient-enriching microbes, particularly nitrogen-fixing bacteria, by the host plant to combat pathogen aggression. This selective increase in nitrogen-fixing bacteria during pathogenesis offers an alternative means of plant defense, boosting the immune response when primary defense mechanisms are compromised. The observed variations in the abundance of nitrogen-fixing bacteria between healthy and infected leaves underscore the intricate interplay between

microbial communities and plant health.

The insights from this study have several implications for developing sustainable disease management strategies. The increased abundance of nitrogen-fixing bacteria such as *Nitrospira* during infection suggests their potential as biocontrol agents. These bacteria can enhance plant health and immune responses, providing a biological alternative to chemical fungicides. Furthermore, beneficial genera such as *Bacillus* and *Pseudomonas*, known for their antifungal properties, could be formulated into microbial inoculants. These inoculants can suppress pathogen growth, maintain microbiota balance, and protect plants against infections. Incorporating beneficial microbes into integrated pest management (IPM) strategies can enhance disease management. Combining microbial inoculants with crop rotation, resistant varieties, and optimized nutrient management can provide a holistic approach, reducing chemical input reliance and minimizing environmental impact.

Further research is required to understand the specific mechanism of plant-microbiome-pathogen interactions, that help in the increased abundance of nitrogen-fixing bacteria. This includes exploring signalling pathways and molecular interactions to develop targeted microbial formulations. Additionally, investigating the synergistic effects of combining multiple beneficial microbes may enhance their protective capabilities, offering robust disease management solutions.

Data availability statement

All data accessed and analyzed in this study are available in the article and its supplementary materials.

CRediT authorship contribution statement

Karun Wilson: Writing – original draft, Visualization, Methodology, Data curation, Conceptualization. **Sathiavelu Arunachalam:** Writing – review & editing, Supervision.

Declaration of competing interest

The authors declare that they have no known competing financial interests or personal relationships that could have appeared to influence the work reported in this paper.

Appendix A. Supplementary data

Supplementary data to this article can be found online at https://doi.org/10.1016/j.heliyon.2024.e37203.

References

[1] B.P.H.J. Thomma, *Alternaria* spp.: from general saprophyte to specific parasite, Mol. Plant Pathol. 4 (2003) 225–236, https://doi.org/10.1046/J.1364-3703.2003.00173.X.

[2] Y. Hou, X. Ma, W. Wan, N. Long, J. Zhang, Y. Tan, S. Duan, Y. Zeng, Y. Dong, Comparative genomics of pathogens causing brown spot disease of tobacco: *Alternaria longipes* and *Alternaria alternata*, PLoS One 11 (2016) e0155258, https://doi.org/10.1371/JOURNAL.PONE.0155258.

[3] P. Adhikari, Y. Oh, D.R. Panthee, Current status of early blight resistance in tomato: an update, Int. J. Mol. Sci. 18 (2017), https://doi.org/10.3390/ijms18102019.

[4] M.T. Brandl, C.E. Cox, M. Teplitski, *Salmonella* interactions with plants and their associated microbiota, Phytopathology 103 (2013) 316–325, https://doi.org/10.1094/PHYTO-11-12-0295-RVW.

[5] C.I. Carlström, C.M. Field, M. Bortfeld-Miller, B. Müller, S. Sunagawa, J.A. Vorholt, Synthetic microbiota reveal priority effects and keystone strains in the *Arabidopsis* phyllosphere, Nat. Ecol. Evol. 3 (2019) 1445–1454, https://doi.org/10.1038/s41559-019-0994-z.

[6] X. Liu, P. Jia, M.W. Cadotte, C. Zhu, X. Si, Y. Wang, F. Chen, J. Wu, S. Zhou, Host plant environmental filtering drives foliar fungal community assembly in symptomatic leaves, Oecologia 195 (2021) 737–749, https://doi.org/10.1007/S00442-021-04849-3.

[7] K.M.G. Dastogeer, F.H. Tumpa, A. Sultana, M.A. Akter, A. Chakraborty, Plant microbiome–an account of the factors that shape community composition and diversity, Curr. Plant Biol. 23 (2020) 100161, https://doi.org/10.1016/J.CPB.2020.100161.

[8] S.L. Woo, F. Scala, M. Ruocco, M. Lorito, The molecular biology of the interactions between *Trichoderma* spp., phytopathogenic fungi, and plants, Phytopathology 96 (2007) 181–185, https://doi.org/10.1094/PHYTO-96-0181.

[9] T.L. Karasov, M. Neumann, A. Duque-Jaramillo, S. Kersten, I. Bezrukov, B. Schröppel, E. Symeonidi, D.S. Lundberg, J. Regalado, G. Shirsekar, J. Bergelson, D. Weigel, The relationship between microbial population size and disease in the *Arabidopsis thaliana* phyllosphere, bioRxiv (2020) 828814, https://doi.org/10.1101/828814.

[10] C.M.J. Pieterse, C. Zamioudis, R.L. Berendsen, D.M. Weller, S.C.M. van Wees, P.A.H.M. Bakker, Induced systemic resistance by beneficial microbes, Annu. Rev. Phytopathol. 52 (2014) 347–375, https://doi.org/10.1146/ANNUREV-PHYTO-082712-102340.

[11] Y. Bai, S. Dong, R. Nishad, T. Ahmed, V. Jasin Rahman, A. Kareem, Modulation of plant defense system in response to microbial interactions, Front. Microbiol. (2020), https://doi.org/10.3389/fmicb.2020.01298.

[12] L.C. Mejía, E.A. Herre, J.P. Sparks, K. Winter, M.N. García, S.A. van Bael, J. Stitt, Z. Shi, Y. Zhang, M.J. Guiltinan, S.N. Maximova, Pervasive effects of a dominant foliar endophytic fungus on host genetic and phenotypic expression in a tropical tree, Front. Microbiol. 5 (2014) 479, https://doi.org/10.3389/FMICB.2014.00479.

[13] I. Vloutoglou, S.N. Kalogerakis, Effects of inoculum concentration, wetness duration and plant age on development of early blight (*Alternaria solani*) and on shedding of leaves in tomato plants, Plant Pathol. 49 (2000) 339–345, https://doi.org/10.1046/J.1365-3059.2000.00462.X.

[14] A. Klindworth, E. Pruesse, T. Schweer, J. Peplies, C. Quast, M. Horn, F.O. Glöckner, Evaluation of general 16S ribosomal RNA gene PCR primers for classical and next-generation sequencing-based diversity studies, Nucleic Acids Res. 41 (2013) e1, https://doi.org/10.1093/NAR/GKS808.

[15] T. Maniatis, E.F. Fritsch, J. Sambrook, J. Engel, Molecular cloning: a laboratory manual. New York: cold spring harbor laboratory. 1982, 545 S., 42, Acta Biotechnol. 5 (1985), https://doi.org/10.1002/ABIO.370050118, 104–104.

[16] S. Andrews, F. Krueger, A. Segonds-Pichon, L. Biggins, C. Krueger, S. Wingett, Babraham Bioinformatics - FastQC: a Quality Control Tool for High Throughput Sequence Data, Fastqc, 2010. https://www.bioinformatics.babraham.ac.uk/projects/fastqc.

[17] P. Ewels, M. Magnusson, S. Lundin, M. Käller, MultiQC: summarize analysis results for multiple tools and samples in a single report, Bioinformatics 32 (2016) 3047–3048, https://doi.org/10.1093/BIOINFORMATICS/BTW354.

[18] C. Quast, E. Pruesse, P. Yilmaz, J. Gerken, T. Schweer, P. Yarza, J. Peplies, F.O. Glöckner, The SILVA ribosomal RNA gene database project: improved data processing and web-based tools, Nucleic Acids Res. 41 (2013) D590–D596, https://doi.org/10.1093/NAR/GKS1219.

[19] T.Z. DeSantis, P. Hugenholtz, N. Larsen, M. Rojas, E.L. Brodie, K. Keller, T. Huber, D. Dalevi, P. Hu, G.L. Andersen, Greengenes, a chimera-checked 16S rRNA gene database and workbench compatible with ARB, Appl. Environ. Microbiol. 72 (2006) 5069–5072, https://doi.org/10.1128/AEM.03006-05.

[20] E.W. Sayers, E.E. Bolton, J.R. Brister, K. Canese, J. Chan, D.C. Comeau, R. Connor, K. Funk, C. Kelly, S. Kim, T. Madej, A. Marchler-Bauer, C. Lanczycki, S. Lathrop, Z. Lu, F. Thibaud-Nissen, T. Murphy, L. Phan, Y. Skripchenko, T. Tse, J. Wang, R. Williams, B.W. Trawick, K.D. Pruitt, S.T. Sherry, Database resources of the national center for biotechnology information, Nucleic Acids Res. 50 (2022) D20–D26, https://doi.org/10.1093/NAR/GKAB1112.

[21] C.E. Shannon, A mathematical theory of communication, Bell Syst. Tech. J. 27 (1948) 379–423, https://doi.org/10.1002/J.1538-7305.1948.TB01338.X.

[22] A. Chao, Nonparametric estimation of the number of classes in a population, Scand. J. Stat. 11 (1984) 265–270. https://www.jstor.org/stable/4615964.

[23] S. Kleine Bardenhorst, M. Vital, A. Karch, N. Rübsamen, Richness estimation in microbiome data obtained from denoising pipelines, Comput. Struct. Biotechnol. J. 20 (2022) 508–520, https://doi.org/10.1016/j.csbj.2021.12.036.

[24] W. McKinney, Data Structures for Statistical Computing in Python, Proc. 9th Python Sci. Conf., 2010, pp. 56–61, https://doi.org/10.25080/majora-92bf1922-00a.

[25] J.D. Hunter, Matplotlib: a 2D graphics environment, Comput. Sci. Eng. 9 (2007) 90–95, https://doi.org/10.1109/MCSE.2007.55.

[26] K.J. Gaston, T.M. Blackburn, J.J.D. Greenwood, R.D. Gregory, R.M. Quinn, J.H. Lawton, Abundance–occupancy relationships, J. Appl. Ecol. 37 (2000) 39–59, https://doi.org/10.1046/J.1365-2664.2000.00485.X.

[27] A. Hagberg, D. Schult, P. Swart, J. Hagberg, Exploring Network Structure, Dynamics, and Function Using NetworkX, 2008.

[28] M. Krzywinski, J. Schein, I. Birol, J. Connors, R. Gascoyne, D. Horsman, S.J. Jones, M.A. Marra, Circos: an information aesthetic for comparative genomics, Genome Res. 19 (2009) 1639–1645, https://doi.org/10.1101/GR.092759.109.

[29] H. Chen, P.C. Boutros, VennDiagram: a package for the generation of highly-customizable Venn and Euler diagrams in R, BMC Bioinf. 12 (2011) 1–7, https://doi.org/10.1186/1471-2105-12-35.

[30] C.H. Dickinson, J.A. Lucas, Plant pathology and plant pathogens, Plant Pathol. 6 (1982).

[31] N. Christian, E.A. Herre, L.C. Mejia, K. Clay, Exposure to the leaf litter microbiome of healthy adults protects seedlings from pathogen damage, Proc. R. Soc. B: Biol. Sci. 284 (2017), https://doi.org/10.1098/RSPB.2017.0641.

[32] J.Y. Cha, S. Han, H.J. Hong, H. Cho, D. Kim, Y. Kwon, S.K. Kwon, M. Crusemann, Y. Bok Lee, J.F. Kim, G. Giaever, C. Nislow, B.S. Moore, L.S. Thomashow, D. M. Weller, Y.S. Kwak, Microbial and biochemical basis of a *Fusarium* wilt-suppressive soil, ISME J. 10 (2016) 119–129, https://doi.org/10.1038/ismej.2015.95.

[33] M.R. Foolad, H.L. Merk, H. Ashrafi, Genetics, genomics and breeding of late blight and early blight resistance in tomato, Crit. Rev. Plant Sci. 27 (2008) 75–107, https://doi.org/10.1080/07352680802147353.

[34] V. Chaudhry, P. Runge, P. Sengupta, G. Doehlemann, J.E. Parker, E. Kemen, Shaping the leaf microbiota: plant–microbe–microbe interactions, J. Exp. Bot. 72 (2021) 36–56, https://doi.org/10.1093/JXB/ERAA417.

[35] M.N.P. Remus-Emsermann, R.O. Schlechter, Phyllosphere microbiology: at the interface between microbial individuals and the plant host, New Phytol. 218 (2018) 1327–1333, https://doi.org/10.1111/NPH.15054.

[36] O.X. Cordero, M.S. Datta, Microbial interactions and community assembly at microscales, Curr. Opin. Microbiol. 31 (2016) 227–234, https://doi.org/10.1016/J.MIB.2016.03.015.

[37] R. Sohrabi, B.C. Paasch, J.A. Liber, S.Y. He, Phyllosphere microbiome, Annu. Rev. Plant Biol. 74 (2023) 539–568, https://doi.org/10.1146/ANNUREV-ARPLANT-102820-032704.

[38] K. Faust, J. Raes, Microbial interactions: from networks to models, Nat. Rev. Microbiol. 10 (8 10) (2012) 538–550, https://doi.org/10.1038/nrmicro2832, 2012.

[39] A. Shade, N. Stopnisek, Abundance-occupancy distributions to prioritize plant core microbiome membership, Curr. Opin. Microbiol. 49 (2019) 50–58, https://doi.org/10.1016/J.MIB.2019.09.008.

[40] A. Shade, J. Handelsman, Beyond the Venn diagram: the hunt for a core microbiome, Environ. Microbiol. 14 (2012) 4–12, https://doi.org/10.1111/J.1462-2920.2011.02585.X.

[41] M. Krzywinski, J. Schein, I. Birol, J. Connors, R. Gascoyne, D. Horsman, S.J. Jones, M.A. Marra, Circos: an information aesthetic for comparative genomics, Genome Res. 19 (2009) 1639–1645, https://doi.org/10.1101/GR.092759.109.

[42] J. Tao, C. Qin, X. Feng, L. Ma, X. Liu, H. Yin, Y. Liang, H. Liu, C. Huang, Z. Zhang, N. Xiao, D. Meng, Traits of exogenous species and indigenous community contribute to the species colonization and community succession, Front. Microbiol. 9 (2018) 3087, https://doi.org/10.3389/FMICB.2018.03087.

[43] J.A. Kyndt, D.M. Salama, T.E. Meyer, Genome sequence of the alphaproteobacterium *Blastochloris sulfoviridis* DSM 729, which requires reduced sulfur as a growth supplement and contains bacteriochlorophyll b, Microbiol. Resour. Announc. 9 (2020) e00313, https://doi.org/10.1128/MRA.00313-20, 20.

[44] S. Zhou, Z. Song, Z. Li, R. Qiao, M. Li, Y. Chen, H. Guo, Mechanisms of nitrogen transformation driven by functional microbes during thermophilic fermentation in an ex situ fermentation system, Bioresour. Technol. 350 (2022), https://doi.org/10.1016/j.biortech.2022.126917.

[45] S.N. Dedysh, W. Liesack, V.N. Khmelenina, N.E. Suzina, Y.A. Trotsenko, J.D. Semrau, A.M. Bares, N.S. Panikov, J.M. Tiedje, *Methylocella palustris* gen. nov., sp. nov., a new methane-oxidizing acidophilic bacterium from peat bogs, representing a novel subtype of serine-pathway methanotrophs, Int. J. Syst. Evol. Microbiol. 50 (2000) 955–969, https://doi.org/10.1099/00207713-50-3-955.

[46] T. Kuhl, S.P. Chowdhury, J. Uhl, M. Rothballer, Genome-based characterization of plant-associated *Rhodococcus qingshengii* RL1 reveals stress tolerance and plant–microbe interaction traits, Front. Microbiol. 12 (2021) 2362, https://doi.org/10.3389/fmicb.2021.708605.

[47] A.S. Bhattacharjee, S. Wu, C.E. Lawson, M.S.M. Jetten, V. Kapoor, J.W.S. Domingo, K.D. McMahon, D.R. Noguera, R. Goel, Whole-community metagenomics in two different anammox configurations: process performance and community structure, Environ. Sci. Technol. 51 (2017) 4317–4327, https://doi.org/10.1021/acs.est.6b05855/suppl_file/es6b05855_si_001.pdf.

[48] B. Zheng, L. Zhang, J. Guo, S. Zhang, A. Yang, Y. Peng, Suspended sludge and biofilm shaped different anammox communities in two pilot-scale one-stage anammox reactors, Bioresour. Technol. 211 (2016) 273–279, https://doi.org/10.1016/j.biortech.2016.03.049.

[49] I.K. Abuley, B.J. Nielsen, Evaluation of models to control potato early blight (*Alternaria solani*) in Denmark, Crop Protect. 102 (2017) 118–128, https://doi.org/10.1016/j.cropro.2017.08.012.

[50] D. Blachinski, D. Shtienberg, A. Dinoor, U. Kafkafi, L.S. Sujkowski, T.A. Zitter, W.E. Fry, Influence of foliar application of nitrogen and potassium on *Alternaria* diseases in potato, tomato and cotton, Phytoparasitica 24 (1996) 281–292, https://doi.org/10.1007/BF02981411.

[51] S.F.A. Shah, B.A. McKenzie, R.E. Gaunt, J.W. Marshall, C.M. Frampton, Effect of early blight (*Alternaria solani*) on healthy area duration and healthy area absorption of potatoes (*Solanum tuberosum*) grown in Canterbury New Zealand with different nitrogen application and stress from potato cyst nematode (*Globodera rostochiensis*), N. Z. J. Crop Hortic. Sci. 32 (2010) 85–102, https://doi.org/10.1080/01140671.2004.9514283.

[52] J.W. Guo, O.A.A. Mohamad, X. Wang, D. Egamberdieva, B. Tian, Editorial: microbiome associated with plant pathogens, pathogenesis, and their applications in developing sustainable agriculture, Front. Microbiol. 15 (2024) 1423961, https://doi.org/10.3389/FMICB.2024.1423961.